Research Article | Vol. 26, No. 17 | 20 Aug 2018 | OPTICS EXPRESS 21574
Optics EXPRESS

Machine learning for 3D simulated visualization of laser machining

DANIEL J. HEATH,[1,*] JAMES A. GRANT-JACOB,[1] YUNHUI XIE,[1] BENITA S. MACKAY,[2] JAMES A. G. BAKER,[2] ROBERT W. EASON,[1] AND BEN MILLS[1]

[1]*Optoelectronics Research Centre, University of Southampton SO171BJ, UK*
[2]*Physics and Astronomy, University of Southampton, Southampton SO17 1BJ, UK*
[*]*djh2v07@soton.ac.uk*

Abstract: Laser machining can depend on the combination of many complex and nonlinear physical processes. Simulations of laser machining that are built from first-principles, such as the photon-atom interaction, are therefore challenging to scale-up to experimentally useful dimensions. Here, we demonstrate a simulation approach using a neural network, which requires zero knowledge of the underlying physical processes and instead uses experimental data directly to create the model of the experiment. The neural network modelling approach was shown to accurately predict the 3D surface profile of the laser machined surface after exposure to various spatial intensity profiles, and was used to discover trends inherent within the experimental data that would have otherwise been difficult to discover.

OCIS codes: (140.3300) Laser beam shaping; (140.3390) Laser materials processing; (100.4996) Pattern recognition, neural networks; (140.7090) Ultrafast lasers; (150.0150) Machine vision.

References and links

1. E. G. Gamaly, A. V. Rode, B. Luther-Davies, and V. T. Tikhonchuk, "Ablation of solids by femtosecond lasers: ablation mechanism and ablation thresholds for metals and dielectrics," Phys. Plasmas **9**(3), 949–957 (2002).
2. B. N. Chichkov, C. Momma, S. Nolte, F. von Alvensleben, and A. Tünnermann, "Femtosecond, picosecond and nanosecond laser ablation of solids," Appl. Phys., A Mater. Sci. Process. **63**(2), 109–115 (1996).
3. M. S. Amer, M. A. El-Ashry, L. R. Dosser, K. E. Hix, J. F. Maguire, and B. Irwin, "Femtosecond versus nanosecond laser machining: comparison of induced stresses and structural changes in silicon wafers," Appl. Surf. Sci. **242**(1–2), 162–167 (2005).
4. O. Albert, S. Roger, Y. Glinec, J. C. Loulergue, J. Etchepare, C. Boulmer-Leborgne, J. Perrière, and E. Millon, "Time-resolved spectroscopy measurements of a titanium plasma induced by nanosecond and femtosecond lasers," Appl. Phys., A Mater. Sci. Process. **76**(3), 319–323 (2003).
5. B. Rethfeld, D. S. Ivanov, M. E. Garcia, and S. I. Anisimov, "Modelling ultrafast laser ablation," J. Phys. D Appl. Phys. **50**(19), 193001 (2017).
6. H. O. Jeschke, M. E. Garcia, M. Lenzner, J. Bonse, J. Krüger, and W. Kautek, "Laser ablation thresholds of silicon for different pulse durations: theory and experiment," Appl. Surf. Sci. **197**, 198839 (2002).
7. J. K. Chen and J. E. Beraun, "Modelling of ultrashort laser ablation of gold films in vacuum," J. Opt. A, Pure Appl. Opt. **5**(3), 168–173 (2003).
8. K. Hornik, M. Stinchcombe, and H. White, "Multilayer feedforward networks are universal approximators," Neural Netw. **2**(5), 359–366 (1989).
9. D. E. Rumelhart, G. E. Hinton, and R. J. Williams, "Learning representations by back-propagating errors," Nature **323**(6088), 533–536 (1986).
10. P. Isola, J. Y. Zhu, T. Zhou, and A. A. Efros, "Image-to-image translation with conditional adversarial networks," arXiv Prepr. 1125– 1134 (2017).
11. S. Amoruso, R. Bruzzese, X. Wang, N. N. Nedialkov, and P. A. Atanasov, "Femtosecond laser ablation of nickel in vacuum," J. Phys. D Appl. Phys. **40**(2), 331–340 (2007).
12. D. J. Heath, J. A. Grant-Jacob, M. Feinaeugle, B. Mills, and R. W. Eason, "Sub-diffraction limit laser ablation via multiple exposures using a digital micromirror device," Appl. Opt. **56**(22), 6398–6404 (2017).
13. D. J. Heath, J. A. Grant-Jacob, R. W. Eason, and B. Mills, "Single-pulse ablation of multi-depth structures via spatially filtered binary intensity masks," Appl. Opt. **57**(8), 1904–1909 (2018).
14. B. Mills, D. J. Heath, M. Feinaeugle, J. A. Grant-Jacob, and R. W. Eason, "Laser ablation via programmable image projection for submicron dimension machining in diamond," J. Laser Appl. **26**(4), 041501 (2014).
15. D. J. Heath, B. Mills, M. Feinaeugle, and R. W. Eason, "Rapid bespoke laser ablation of variable period grating structures using a digital micromirror device for multi-colored surface images," Appl. Opt. **54**(16), 4984–4988

#330860 https://doi.org/10.1364/OE.26.021574
Journal © 2018 Received 3 May 2018; revised 8 Jun 2018; accepted 28 Jun 2018; published 7 Aug 2018

Optics EXPRESS

(2015).
16. Zygo, "Optical Profiler Basics," https://www.zygo.com/?/met/profilers/opticalprofilersabout.htm.
17. P. Y. Simard, D. Steinkraus, and J. C. Platt, "Best practices for convolutional neural networks applied to visual document analysis," Seventh Int. Conf. Doc. Anal. Recognition, 2003. Proceedings. **1**(Icdar), 958–963 (2003).
18. O. Ronneberger, P. Fischer, and T. Brox, "U-net: convolutional networks for biomedical image segmentation," in *Medical image computing and computer-assisted intervention–miccai 2015*, N. Navab, J. Hornegger, W. M. Wells, and A. F. Frangi, eds. (Springer International Publishing, 2015), pp. 234–241.
19. J. A. Grant-Jacob, S. J. Beecher, J. J. Prentice, D. P. Shepherd, J. I. Mackenzie, and R. W. Eason, "Pulsed laser deposition of crystalline garnet waveguides at a growth rate of 20 μm per hour," Surf. Coatings Technol. **84**(22), 4502–4504 (2018).
20. S. Amoruso, R. Bruzzese, N. Spinelli, R. Velotta, M. Vitiello, X. Wang, G. Ausanio, V. Iannotti, and L. Lanotte, "Generation of silicon nanoparticles via femtosecond laser ablation in vacuum," Appl. Phys. Lett. **343**, 7–10 (2004).
21. J. A. Grant-Jacob, B. Mills, and R. W. Eason, "Parametric study of the rapid fabrication of glass nanofoam via femtosecond laser irradiation," J. Phys. D Appl. Phys. **47**(5), 055105 (2014).
22. A. F. Courtier, J. A. Grant-Jacob, R. Ismaeel, D. J. Heath, G. Brambilla, W. J. Stewart, R. W. Eason, and B. Mills, "Laser-based fabrication of nanofoam inside a hollow capillary," Mater. Sci. Appl. **08**(12), 829–837 (2017).
23. J. H. Yoo, J. B. Park, S. Ahn, and C. P. Grigoropoulos, "Laser-Induced direct graphene patterning and simultaneous transferring method for graphene sensor platform," Small **9**(24), 4269–4275 (2013).
24. D. J. Heath, M. Feinaeugle, J. A. Grant-Jacob, B. Mills, and R. W. Eason, "Dynamic spatial pulse shaping via a digital micromirror device for patterned laser-induced forward transfer of solid polymer films," Opt. Mater. Express **5**(5), 1129 (2015).
25. M. Feinaeugle, D. J. Heath, B. Mills, J. A. Grant-Jacob, G. Z. Mashanovich, and R. W. Eason, "Laser-induced backward transfer of nanoimprinted polymer elements," Appl. Phys., A Mater. Sci. Process. **122**(4), 398 (2016).
26. R. C. Y. Auyeung, H. Kim, S. Mathews, and A. Piqué, "Laser forward transfer using structured light," Opt. Express **23**(1), 422–430 (2015).
27. S. A. Mathews, R. C. Y. Auyeung, H. Kim, N. Charipar, and A. Piqué, "High-speed video study of laser-induced forward transfer of silver nano-suspensions," J. Appl. Phys. **114**(6), 064910 (2013).

1. Introduction

The physical processes that govern laser machining of a surface are particularly complex, including not only the light-matter interactions that transfer energy to the sample surface, but subsequent heat conduction, phase-changes of the sample material, dynamics of material in non-solid phases, re-deposition of material and so on [1–4]. The exact evolution of these processes will depend on many factors, including the sample type, as well as the particular intensity profile incident on the sample surface, which itself may have undergone diffractive effects that must be considered. In the case of laser machining using a pulsed laser source, the temporal interaction of the laser energy with the sample surface must also be taken into account, as different interaction effects become dominant for different pulse lengths and intensities. In the case of femtosecond pulses, where the removal mechanism is highly nonlinear and can include ionization as well as melting, the complexity is further increased. Whilst others [5–7] have started from photon-atom interactions, the highly nonlinear nature of the processes means that accurate predictions over larger areas are challenging, due in part to nonlinear demands on computing power as the number of atoms is increased.

Rather than starting from fundamental physical processes and scaling up to simulate the effect of laser machining at experimentally useful size scales, the technique presented in this paper follows an empirical approach; starting from experimental data to model laser-machined surface profiles after exposure to various spatially shaped laser intensity patterns. This approach is achieved via the use of a neural network (NN) that is trained on experimental images of laser machined surfaces, and which subsequently encodes a description of the laser machining processes. As shown here, the trained NN can then be used to simulate the experiment and hence predict the 3D surface profile that would result from laser machining of the material surface with previously unobserved intensity profiles. Whilst here the NN was trained to predict the 3D surface after three exposures of identically spatially shaped ultrafast pulses, this approach could be extended to non-identical pulses, or a continuous wave laser source, with appropriate training data. Three pulses were chosen in this work to ensure a high contrast in depths of machining.

Optics EXPRESS

The concept demonstrated in this paper, as shown in Fig. 1, was to train a NN to transform a two-level (on or off) laser spatial intensity profile into a 3D surface profile of the laser machined surface. Rather than constructing a model from first principles, this NN approach required a data set of experimental images of the material surface when machined with a random selection of spatial intensity profiles. Therefore, this demonstration also offers a template for the modelling of other experimental systems where the underlying processes are unknown or are too complicated to model accurately.

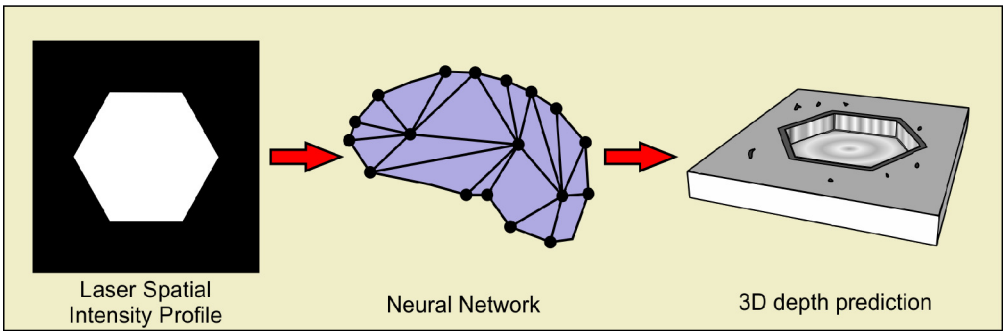

Fig. 1. Concept diagram of transforming a laser spatial intensity profile into a predicted 3D surface profile of the laser-machined surface, via a neural network. The input to the neural network was a laser spatial intensity profile, and the output was the predicted 3D laser-machined surface profile. Added in the conceptual depth prediction are an imperfect flatness at the bottom of the machined structure, raised lip, or burr, around the perimeter, and redeposited debris, all typical of laser machining.

2. Neural networks

NNs [8] are a set of algorithmic systems that are created as an interconnected network of neurons, where each neuron receives, processes and then outputs information. Typically, a NN is formed of an input layer, a series of hidden layers, and an output layer. A NN can therefore be considered as a transfer function that maps information from an input domain onto an output domain. Rather than rigorously being programmed with exact representations of relevant processes, such as optical diffraction or melting effects, or even being instructed to search specifically for such representations, the NN takes a holistic approach – generating a transfer function that represents the combination of the physical processes occurring. In general, this internal representation is encoded via use of an algorithmic training procedure known as backpropagation [9], in which the weightings between the neurons are automatically modified. The training process requires a set of experimental data, known as the training data set, which contains input data and the associated output data. In this paper, the input data was a set of bitmap patterns uploaded to a spatial light modulator, used to spatially shape laser intensity profiles, and the output data was experimentally measured height profiles of the laser machined surface. During training, the NN was provided with input bitmap patterns used in the laser machining experiment, which it processed, and then produced a predicted surface height profile. The predicted output from a particular input bitmap was compared to the experimentally measured output for the corresponding input bitmap from the training data set, and the difference (i.e., the error) was determined. This error was propagated backwards through the NN, and the weightings of the neurons changed accordingly, and consequently the error was reduced for subsequent iterations.

This work used a NN variant known as a conditional adversarial network (CAN) [10], which is particularly effective at discovering correlations and patterns within image data. This particular NN variant has the additional benefit that it can be trained to produce output data that is near-indistinguishable from data in the training data set [10]. A hierarchical series of convolutional processes occur within the network, which can enable the identification of the features that exist in the image data. During training, these convolutional processes are

Optics EXPRESS

automatically optimized in order to encode the transformation of features from the input domain to the output domain. The section of the NN devoted to this is known as the encoder-decoder, while an additional section known as the 'discriminator' is trained to determine genuine results from computer-predicted ones. The encoder-decoder is then trained to both learn the transformation from input to output domains and to 'fool' the discriminator into judging predicted results as genuine. It is the presence of the discriminator which allows the NN to produce realistic features, rather than being trained to produce an 'average' result which may appear blurred. While an average result may capture many features of laser machining, other details may be difficult to discern: the distribution of debris and corrugation of burr for instance. In particular, the minimum resolution machined in a given structure would be difficult to predict from a blurred output. It is for this reason that the CAN architecture was chosen. The result is that the NN was able to encode a transformation that was dependent on the specific features present in the spatial intensity profile, as well as predicting realistic distributions of probabilistic detail, such as debris. The NN architecture was based on previous work [10] that was extended to a 512 by 512 pixel resolution using an additional convolutional layer.

3. Experimental setup, data collection, and neural network training

A fundamental requirement of training a NN is the collection of an appropriate training data set. Here, the goal was to train a NN to convert a chosen spatial intensity profile into the associated 3D surface profile of the laser-machined surface. To achieve this, two experimental components were required. Firstly, a laser machining setup, which provided control over the spatial intensity profile of the incident laser pulses. Secondly, a characterization setup, which could accurately measure the 3D surface profile of the sample after machining. The experimental schematics, along with three examples from the training data set are shown in Fig. 2. In the figure, the experimental 3D depth profiles show negative/positive values in nanometers, where positive values correspond to recast debris and burr. The background height of the sample was set to 0 nm height, and to make visual comparisons between predicted surface profiles easier, the color bars in the figure is limited between 150 nm and –300 nm.

Optics EXPRESS

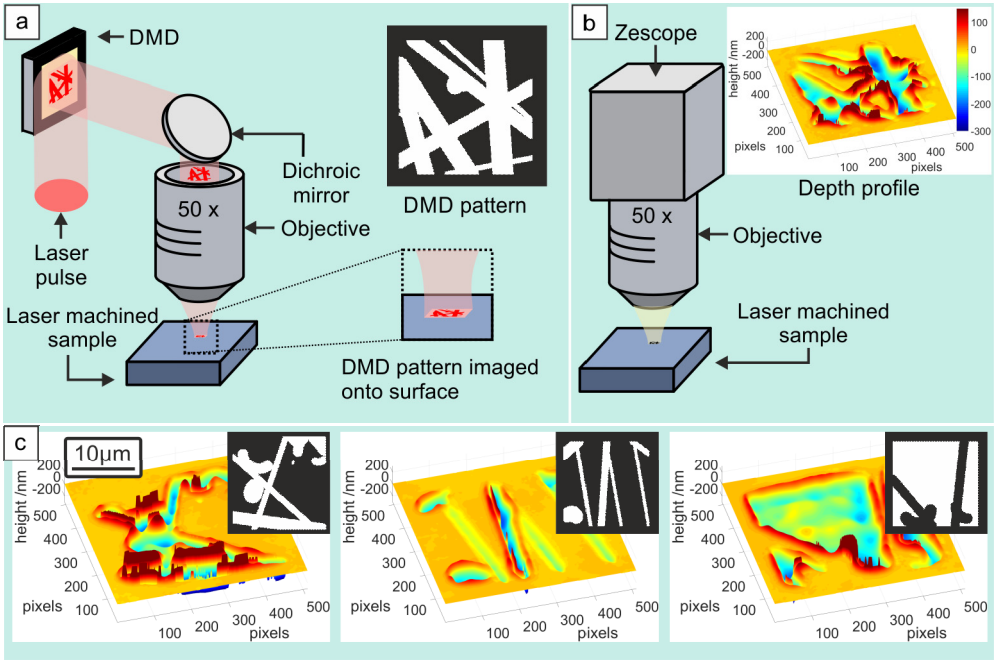

Fig. 2. Experimental approaches for collecting appropriate training data, along with training data examples. Showing a) schematic of the laser machining setup, b) illustration of the sample characterisation method, and c) three examples from the training data set.

The laser machining setup used a digital micromirror device (DMD), acting as an intensity spatial light modulator, to spatially shape single 150 fs, 800 nm, 1 mJ laser pulses from a Ti:sapphire amplifier. The pulses were attenuated and spatially homogenised (via a πShaper 6_6) such that a uniform fluence of 2.8 mJ/cm^2 was incident on the DMD surface. The shaped laser pulses were then imaged onto the target sample using a 50x objective, which increased the fluence to a level suitable for laser machining (in this case 1.8 J/cm^2, a fluence comparable to that found for efficient material ejection by others [11]). The DMD was aligned such that a spatial intensity pattern corresponding to the layout of on (white in figures) or off (black in figures) pixels would be directed towards the sample. The capabilities of this experimental setup have been extensively discussed elsewhere [12–15]. The sample was an electroless nickel mirror (5 µm electroless nickel layer deposited on copper, LBP Optics Ltd.), which had an amorphous structure and was chosen to reduce grain boundary effects. The DMD patterns used for the training data set were generated by randomly combining lines and segments of circles. The 3D surface profiles were measured interferometrically using a Zygo Zescope, accurate to below 1 nm depth measurements [16]. Each lateral pixel in the depth profiles presented in this paper correspond to a distance of 64 nm (though optical resolution on the detector was of order 500 nm), with each structure being approximately 30 µm across. A total of 165 data set pairs were created, similar to those in Fig. 2(c), and used for training. The training data set was augmented from 165 to 5000 images via random translation of the data in each training data set item [17]. The NN operated at a resolution of 512 by 512 pixels, and was trained for 100 epochs (where one epoch is defined as training on all 5000 images exactly once, and one iteration is defined as training on a single image) with a learning rate of 0.0003, batch size of 1, and total time of 3 days. The network was based on an encoder-decoder architecture, with 17 layers, and stride of 2, a 4 by 4 kernel size, and used a rectified linear unit activation functions, hence taking the image size from 512 by 512, down to 2 by 2, then back up to 512 by 512. The encoder-decoder was based on a U-net structure [18], with skip connections between the mirrored layers. The discriminator

Optics EXPRESS

was formed of 4 layers of convolutional processes with stride of 2, taking the image size from 256 by 256 down to 32 by 32, leading to a single output, via a sigmoid activation function that labelled realistic or unrealistic.

4. Neural network validation

In order to test the NN accuracy on real-world data, a data set that is separate to the training data set is generally collected. In this case this separate data set, known as the validation data set, was not used during training, and hence offered a test of the trained NN on unseen data. However, the validation data set was collected experimentally within the same time window as the training data. Two examples of input images (a high intensity white 'X' on a zero intensity black background, and an intensity-inverted 'X' – a black 'X' on a white background) from the validation data set are shown in Fig. 3.

The surface profile predicted by the NNs after a series of training iterations, based on these inputs, are shown, to demonstrate the improvement achieved via backpropagation, where the figure shows (a) 50, (b) 5000, and (c) 50000 training iterations. In order to demonstrate the role of the discriminator, the top two rows in Fig. 3 show the output from a NN trained while the effect of the discriminator is turned off, and the bottom two rows show the output when the NN is trained with the discriminator on. When the influence of the discriminator is removed during training, the CAN architecture is effectively reduced to a *convolutional neural network* (CNN), a common architecture in image processing NNs.

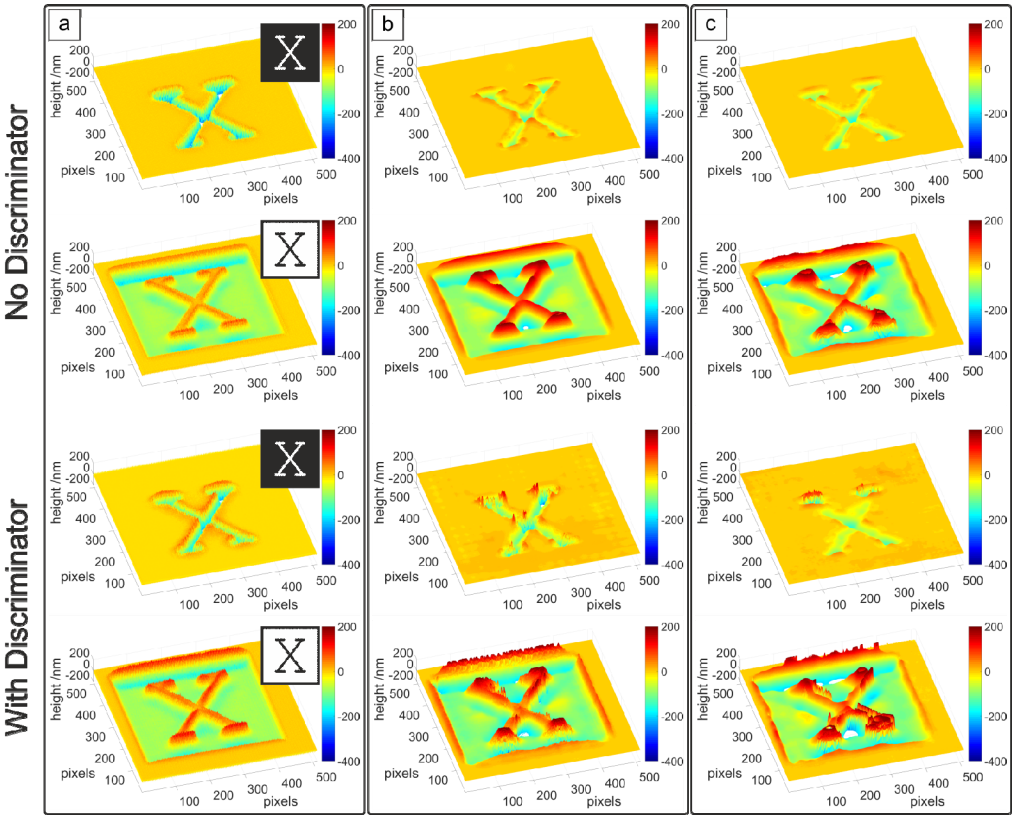

Fig. 3. Predicted surface profiles from both a CNN architecture (no discriminator, top two rows) and a CAN architecture (with discriminator, bottom two rows) after a) 50, b) 5000, and c) 50000 training iterations, showing distinct improvements in appearance. Training on each single image took about 250 milliseconds. Insets in (a) show the input bitmaps used by the NNs to predict the depth profiles.

Optics EXPRESS

The results in Fig. 3(a) are clearly distinguishable from the appearance of the experimentally measured results in Fig. 2(c). While the CAN outputs, in the bottom two rows, show raised burr at the perimeter interface between regions exposed and not exposed to the shaped intensity profile at this point of training (albeit overly uniform), as occurs in real laser machining, the CNN output shows little to no burr. Both sets of profiles improve, however, in Fig. 3(b), after 5000 training iterations. The CNN and CAN have introduced realistic non-flat bottoms to the machined structures, and the CNN has begun predicting burr. The CAN at this point has moved on to introducing non-uniformity to the burr, as well as scattered debris (evident on the background region of the machined 'X'). In Fig. 3(c), the CAN has introduced yet more realistic non-uniformity to the burr, as well as distributing debris in a less ordered manner, both appearing consistent with real laser machining profiles, as will be seen in Fig. 4. The CNN, however, has failed to predict any noticeable debris after 50000 training iterations, and little change to the uniformity of burr has been made. With this in mind, the CAN architecture has been used for the remainder of this work.

Figure 4 shows the remarkable similarity between predicted profiles in Fig. 4(a) and 4(c) compared with the experimentally measured 3D surface profiles in Fig. 4(b) and 4(d), after 100 epochs (i.e., after training on all 5,000 images 100 times). The NN is clearly seen to accurately predict the depth, width, and even the cross-sectional profile of laser machined features. Features that are challenging to predict via analytical approaches, such as the height of burr, depth variations, and average depth are accurately reproduced.

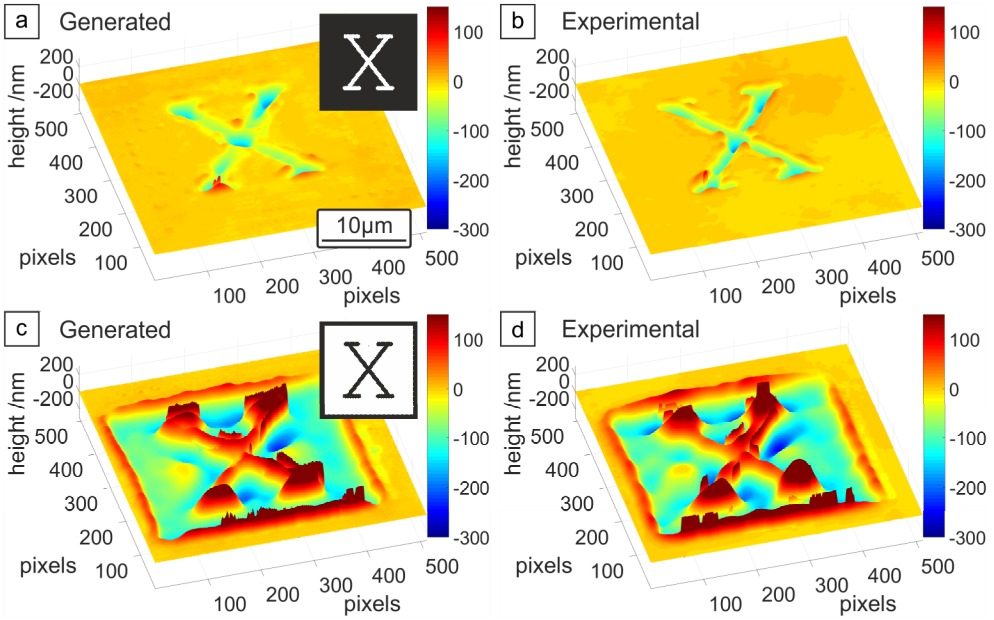

Fig. 4. Comparison of generated and experimentally measured images for spatial intensity patterns shaped into the letter 'X' in (a) and (b) respectively, and an inverted intensity 'X' in (c) and (d). Clear similarities are observed for both cases, in particular the depth, width and profile of the laser machined features, along with analytically difficult to predict features, such as burr height.

The small differences between the predicted and experimentally measured profiles are attributed predominantly to each experimentally measured image corresponding to a single result produced on an experimental setup that was subject to random noise, such as fluctuations of the laser pulse energy or inhomogeneities of the sample. The NN output represents the outcome for the given encoding of the entire training data set, and so the effect of random fluctuations applied by the NN to an unseen input may differ from those present

Optics EXPRESS

when that input was used to predict experimental data for validation. Nonetheless, the NN has produced an extremely realistic result.

5. Predictive analytics via the trained neural network

The trained NN offers significant potential for predictive capabilities, as it can be used to produce the 3D surface profile that would likely result from laser machining using a wide variety of spatial intensity profiles, including, of particular interest, ones not used in the experiment that generated the training data. For the NN used here, the transformation from intensity profile to 3D surface profile typically took 250 milliseconds. Therefore, it was feasible to use this approach to predict the output for a large number of spatial intensity profiles and subsequently analyze the predicted 3D surface profiles to discover experimental trends that would otherwise have been onerous to collect. This approach can therefore also be considered as a method for reorganizing experimental data into a format more appropriate for human interpretation. For instance, suppose a relationship between the width of a projected circular intensity profile and machining depth was desired. Previously, an obvious way to investigate this relationship would be to use the DMD to project a series of incrementally larger circles at a sample, measure each depth, and determine an empirical relationship. Such a relationship is sought in Fig. 5 and Fig. 6, which used over 200 data points. This experiment would, indeed, take a roughly equivalent time to perform as the generation of the training data in this work, which contained 167 data points before automated augmentation. However, supposing the same relationship for projected square beam profiles of different sizes, or triangular profiles, was desired – an equally lengthy experiment and analysis would be required for each. Though there is an initial time cost in training the NN, almost no human labor is required, compared with the effort and specialized equipment required in aligning and characterizing a sample via the optical setup and profilometer, if each empirical relationship were sought through new experiments. With the trained NN, programmatically-generated input intensity profiles can be rapidly associated with likely output depth profiles. Rather than requiring additional experiments for each shape of beam profile, a likely empirical relationship can be found without further use of a laser, or indeed access to samples. The NN has effectively collated most, if not all, salient information to be gleaned from the collected data, and allows creative interrogation by a user. Such an interrogation is demonstrated below, to find a relationship between projected circular intensity profile diameter and depth of machining.

Figure 5 shows the result of using the NN to simulate laser machining with a circular spatial intensity with various diameters. Figure 5(a)–5(d) shows the predicted 3D surface profile along with associated radially averaged cross sectional profiles, for diameters of 1, 3, 5, and 7 μm respectively. As expected, the width of the machined features increases as the beam size is increased. However, the relationship between beam size and maximum depth is not monotonic, but rather the maximum depth is seen to decrease in value for beam diameters larger than approximately 3 μm.

Optics EXPRESS

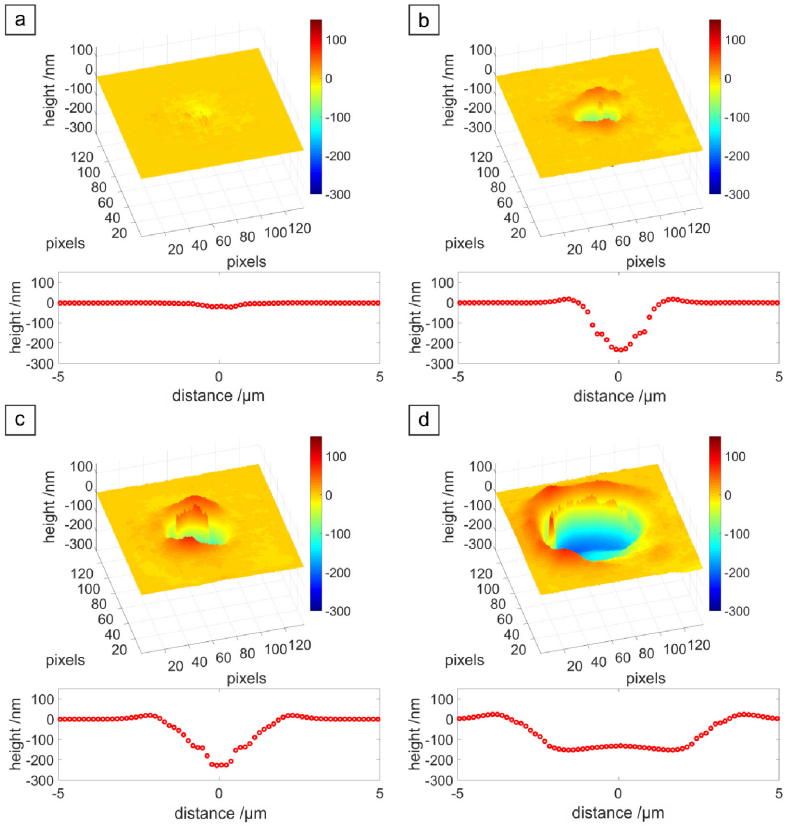

Fig. 5. Predicted output from the NN when machining with a circular top-hat beam with diameter a) 1 μm, b), 3 μm, c) 5 μm and d) 7 μm, along with the radial averages of the profiles shown below each 3D profile.

In order to investigate this relationship between beam size and machined depth, and to determine a physical cause, the expected intensity profiles after optical filtering through a simulated aperture at the Fourier plane were calculated (as in [13]). The resulting central intensity (in arbitrary units) with two simulated aperture lateral positions are plotted in Figs. 6(a) and 6(b) respectively, and the depth of machining at the centre of the features as predicted by the NN is plotted in Fig. 6(c).

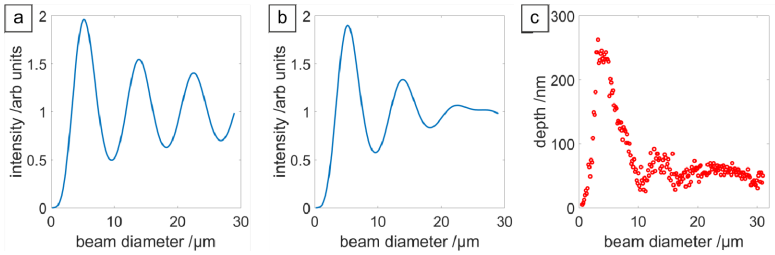

Fig. 6. Calculated intensity at the central position on the sample as a function of beam diameter, as predicted by an optical filtering model in (a) and (b) and laser-machined depth predicted by the NN in (c). The optical filtering model predicts the intensity and the NN predicts the depths of machining. The simulated aperture used for optical filtering in (a) was shifted from a central position laterally by an amount corresponding to ~28 μm in the experiment to produce (b), and consequently more closely matches (c) than does (a), suggesting a previously unknown optical misalignment on the laser machining setup, discovered owing to the interrogation of the trained NN.

Optics EXPRESS

There will be some correspondence between the intensities predicted and the machining depths, though the additional physical effects mentioned in Section 1 would likely need to be included for an analytical model to accurately predict depth. Nonetheless, a maximum intensity at a beam diameter of ~5 µm is indeed discovered when accounting for optical filtering, in Fig. 6(a), showing some agreement with the NN predictions in Fig. 6(c) if increased intensity is assumed to result in increased depth. However, the modulation ratio of oscillations in Fig. 6(a) appear large compared to those in Fig. 6(c), and appear to cease after a beam diameter of 20 µm. The NN model then, appears to be accounting for additional effects. A misalignment with the aperture at the Fourier plane was introduced, a lateral shift which corresponded to ~28 µm misalignment, to produce Fig. 6(b), which show closer agreement with output from the NN model, showing smaller oscillations after the initial turning point in central depth, and almost no oscillation after 20 µm beam diameter in maximum depth.

From this analysis, it appears that the NN had encoded the existence of a previously unrecognized misalignment on the laser machining setup. Though this phenomena *can* be explained analytically, as above, the flaw in the beamline would be unlikely to be discovered, much less explained, without the ability to rapidly interrogate the trained NN.

To demonstrate the capability of the NN for analytics on further machining features, Fig. 7 shows the predicted amount of material removed from the machined feature along with the amount of material recast as debris in the surrounding area, for various beam diameters. This was calculated by summing up the negative and positive pixel values in each predicted output, corresponding to removed and added material respectively. The percentage of material that is recast as debris is shown in Fig. 7(b), which shows a peak for a beam diameter around 5 µm corresponding to approximately 30% of material removed ending up as debris. This percentage decreases for larger diameters.

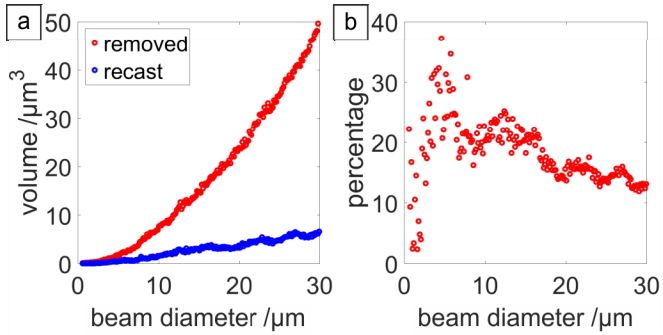

Fig. 7. Further analytics generated via interrogation of the NN output: a) volume of removed material, and recast material as debris in the surrounding area, and b) percentage of removed material that is recast as debris.

The information in Fig. 7 may be invaluable, depending on the needs of the laser process at hand. In pulsed laser deposition [19], any redeposited material on the original substrate is wasted, and hence minimizing this would lead to a more efficient process. Similarly, it is rarely advantageous to contaminate the surrounding material surface, or previously machined structures, with debris. If a 5 µm wide feature were to be machined, without the above information one might choose to machine the entire feature in a single exposure. However, if redeposited debris were a concern, Fig. 7(b) demonstrates that it may be better to stitch several 1 µm wide exposures together to form a final pattern. Conversely, in the production of nanofoam and other nanoparticles for instance [20–23], redeposited material is vital to the process, and selecting a beam size to maximize this would be beneficial. Further, laser-induced transfer processes [24–27] may aim for parity between ejected and redeposited material from and to respective substrates.

Optics EXPRESS

This technique is therefore suitable for training on any laser process where a final surface profile is measurable, and is of interest. It could be used for the rapid testing of new control parameters, optimization, and diagnosis of faults, all without the requirement of additional laboratory testing.

6. Conclusions

We have demonstrated that an NN can be used to simulate the depth profile resulting from laser machining using previously untested spatial intensity profiles, directly from processing limited experimental data. Rather than requiring a systematic exploration of a particular feature type in the intensity profiles, such as parallel lines of different thicknesses and separations, or crossed lines meeting at a series of angles, a set of only 165 randomly generated spatial intensity profiles was sufficient for the NN to predict realistic results for unseen profiles. This is in contrast to the analytical approach of building up a model from first-principles, which can be challenging or even impossible to accurately scale up to experimentally useful sizes. The NN approach has the significant advantages of requiring zero understanding of the underlying physical processes and also being able to encode experimental quirks that might not have been possible to include in a purely analytical model (such as a misaligned beam in this case, which was an unknown factor at the time of experiment). This approach allows the extraction of experimental relationships and properties that might have otherwise remained hidden in the original experimental data. The NN therefore also acts as a powerful statistical device for discovering relationships between experimental parameters, as it effectively enables the reorganization of experimental data into a format more appropriate for human interpretation. This approach could enable modelling in challenging optical and physical systems and lead to the discovery of new relationships between parameters existing in experimental data.

Funding

Engineering and Physical Sciences Research Council (EPSRC) (EP/N03368X/1, EP/N509747/1).

Acknowledgments

We gratefully acknowledge the support of NVIDIA Corporation with the donation of the Titan X GPU used for this research. Supporting data for this submission can be found at https://doi.org/10.5258/SOTON/D0514.